Out-of-field dose assessment for a 1.5 T MR-Linac with optically stimulated luminescence dosimeters

Yan Zhang
School of Physics and Technology, Wuhan University, Wuhan, P.R. China
Department of Radiation Oncology Physics and Technology, Shandong Cancer Hospital and Institute, Shandong First Medical University and Shandong Academy of Medical Sciences, Jinan, P.R. China

Shaojie Yan
Department of Radiation Oncology Physics and Technology, Shandong Cancer Hospital and Institute, Shandong First Medical University and Shandong Academy of Medical Sciences, Jinan, P.R. China
School of Nuclear Science and Technology, University of South China, Hengyang, P.R. China

Zhen Cui, Yungang Wang, Zhenjiang Li and Yong Yin
Department of Radiation Oncology Physics and Technology, Shandong Cancer Hospital and Institute, Shandong First Medical University and Shandong Academy of Medical Sciences, Jinan, P.R. China

Baosheng Li
Department of Radiation Oncology, Shandong Cancer Hospital and Institute, Shandong First Medical University and Shandong Academy of Medical Sciences, Jinan, P.R. China

Hong Quan[a)]
School of Physics and Technology, Wuhan University, Wuhan, P.R. China

Jian Zhu[a)]
Department of Radiation Oncology Physics and Technology, Shandong Cancer Hospital and Institute, Shandong First Medical University and Shandong Academy of Medical Sciences, Jinan, P.R. China
Shandong Medical Imaging and Radiotherapy Engineering Center, Jinan, P.R. China
Shandong Key Laboratory of Digital Medicine and Computer Assisted Surgery, The Affiliated Hospital of Qingdao University, Qingdao, P.R. China

(Received 18 November 2020; revised 4 February 2021; accepted for publication 4 March 2021; published 10 May 2021)

Purpose: To assess the out-of-field surface and internal dose of the 1.5 T MR-Linac compared to the conventional external beam linac using optically stimulated luminescence dosimeters (OSLDs), and evaluate the out-of-field dose calculation accuracy of the Monaco treatment planning system (TPS) of the 1.5T MR-Linac.

Methods: A cubic solid water phantom, with OSLDs on the surface, was vertically irradiated by MR-Linac square fields with different sizes. In addition, OSLDs were arranged out of the beam edges in four directions. An anthropomorphic adult phantom, with 125 cm^3 simulated volume, was irradiated in four orthogonal directions by both MR-Linac and conventional linac at the head, thoracic, and pelvic sites. Out-of-field doses were measured by OSLDs on both the surface and internal emulational organs at risk (OARs). The results were compared to the simulated dose from Monaco TPS.

Results: At different field sizes (5×5 to 20×20 cm^2) and distances (1 to 10 cm) to beam edge, the out-of-field surface dose measured on MR-Linac varied from 0.16 % (10 cm to 5×5 cm^2 edge) to 7.02 % (1 cm to 20×20 cm^2 edge) of the maximum dose laterally and from 0.14 % (10 cm to 5×5 cm^2 edge) to 8.56 % (1 cm to 20×20 cm^2 edge) of the maximum dose longitudinally. Compared to the OSLDs measured data, the Monaco TPS presented an overestimate of the out-of-field dose of OARs at 0–2 % isodose area on both surface and internal check points, and the overestimation gets greater as the distance increases. The underestimation was found to be 0–35% at 2–5% isodose area on both surface and internal check points. Compared to the conventional linac, MR-Linac delivered higher average values of out-of-field dose on surface check points (20%, 19%, 21%) and internal simulated OARs (42%, 37%, 9%) of the anthropomorphic phantom at head, thoracic, and pelvic irradiations, respectively.

Conclusions: Compared to the conventional linac, MR-Linac has the same out-of-field dose distribution. However, considering the absolute dose values, MR-Linac delivered relatively higher out-of-field doses on both surface and internal OARs. Additional radiation shielding to patients undergoing MR-Linac may provide protection from out-of-field exposure. © *2021 The Authors. Medical Physics published by Wiley Periodicals LLC on behalf of American Association of Physicists in Medicine* [https://doi.org/10.1002/mp.14839]

Key words: anthropomorphic phantom, MR-Linac, OSL dosimeters (OSLDs), out-of-field dose

1. INTRODUCTION

With the advent of upgraded radiation accelerators, manifold radiation technologies, and improvements in imaging guidance technology, image-guided radiation therapy (IGRT) was introduced for highly targeted tumor location, high-resolution tumor boundary delineation, and accurate treatment delivery.[1] Cone-beam computed tomography is recognized in widespread applications as it modifies the patient position error appropriately before treatment; however, it has several drawbacks such as poor image quality and severe shading of artifacts owing to extra scatter radiation.[2,3] To further reduce the limitations of image quality for the development of radiotherapy, the concept of combining an MRI scanner with a linear accelerator has been developed, termed as MR-Linac. By providing the benefits of superior soft-tissue contrast, nonradiative exposure, and real-time anatomical image tracking for routine adaptive strategies, the MR-Linac achieves good recognition for clinical practice.[4,5]

However, the effects of the magnetic field on dose perturbations in practice have raised concerns. Owing to the two beam-field systems in the design of the MR-Linac,[6] the two orientations of the magnetic field, with respect to the radiation beam, influence the dose perturbation caused by the secondary electrons in different ways. For the magnetic field parallel to the radiation beam, electrons produced by the Linac head or air move straight along the direction of the radiation beam with less lateral scattering. For the targets that are close to the patient surface or in some low density tissues, the electrons strike the patient and finally are deposited on the surface, which increases the planning target volume (PTV) dose. To an extent, this spares the neighboring normal tissues.[7,8] For the transverse magnetic field, there is a lateral shift of profiles in the direction of the Lorentz force and a decrease in the depth of the maximum dose.[9] Additionally, the electron return effect occurs between interfaces of different densities.[10,11] Nachbar et al. identified that the out-of-field electron stream effect (ESE) dose could be accurately calculated by the treatment planning system (TPS).[12] Park et al. reported that an unwanted electron stream is observed outside the treatment region in partial breast irradiation in the presence of the magnetic field.[13] Moreover, Hackett et al. determined that the contaminant electrons are within the same order of magnitude as the scattered or leaked photons for larger fields.[14]

These studies have shown the non-negligible impact of the magnetic field on secondary electrons, which induces extra dose deposition outside the target volume. In addition, out-of-field scattered photons should also be investigated for the MR-Linac. The out-of-field dose is relatively low; however, most secondary cancers occur in the proximity of the targeted volume.[15] Organs at risk (OARs), especially radiosensitive organs (i.e., eyes, thyroid, breasts, and gonads) which surround the irradiation region, are inevitably exposed to radiation, which may increase the risk of deleterious effects and even secondary malignancy.[16] Tubiana et al. reported that doses as low as 10 cGy in pediatric radiotherapy could lead to thyroid and breast malignancies.[17] The threshold dose for radiation-induced cataract formation may be less than 0.5 Gy[18] with a linear no-threshold model.[19,20] Thus, for pediatric patients, a low level of radiation exposure can lead to many side effects.[21,22] As mentioned above, it is important to investigate and quantify the out-of-field dose in the magnetic field.

Owing to the original configurations of the MR-Linac and the complexity of out-of-field dose distribution, there is minimal literature focusing on the out-of-field dose distribution of the MR-Linac, and it remains to be investigated and measured using reliable dosimeters. It has been proven that optically stimulated luminescence dosimeters (OSLDs) are MR-safe detectors.[23] In addition, the beryllium oxide material, used in an OSLD, possesses favorable features, such as near tissue equivalence ($Z_{eff} = 7.2$),[24] high sensitivity, wide linearity range, and low energy dependence.[25] Hence, OSLDs can accurately measure the dose in a magnetic field.[26]

At the same time, there are several published works identifying the poor performance, including under- and overestimation, of out-of-field dose calculation of specific TPSs.[27–29] However, the accuracy of out-of-field dose calculation of the Monaco TPS, including the Graphics Processing Unit-based Monte Carlo dose calculation algorithm (GPUMCD) in the magnetic field, has rarely been evaluated.

This study aims to assess the out-of-field surface and internal dose of the 1.5 T MR-Linac compared to the conventional external beam linac using OSLDs, and evaluate the out-of-field dose calculation accuracy of the Monaco TPS of the 1.5 T MR-Linac.

2. MATERIALS AND METHODS

2.A. Optically stimulated luminescence dosimeters

The OSLD system (RadPro International GmbH, Germany) is composed of several myOSLchips; a handheld manual OSL reader; an eraser with 24 blue power light-emitting diodes for annealing; and software for registration, calibration, and measurement. Similar to nanoDot dosimeters (Landauer, Illinois, USA), OSLDs are made from beryllium oxide (BeO) and have a sensitive area of 4.7×4.7 mm^2 embedded into a hard-plastic holder, with a QR code and number labels for identification. Each dosimeter has a total length, width, and thickness of 1 cm, 1 cm, and 2 mm, respectively. Annealing each chip after the measurement is of great importance because it eliminates the effects of accumulated signals.

2.A.1. Calibration

Based on the guideline proposed by the vendor, preprocessing is essential for the OSLDs before use. A batch of OSLDs was preirradiated with a 10 Gy dose to improve stability. After removing the plastic casings, the BeO chips were annealed by an eraser for more than 4 h. After registration was completed, another important procedure was the calibration of the OSLDs based on the conventional Linac, which

was then passed through the daily quality assurance protocol. Several high-performance dosimeters were selected for calibration mode as reference dosimeters, and the rest were switched to field mode for use.

The three steps of the calibration were implemented in sequence. First, the background values of OSLDs were read by the manual OSL reader; then, they were positioned on the linac couch between two solid water slabs, which were used for buildup and backscatter. After irradiation with a known local exposure value under the 6 MV beam, the OSLDs were placed in the reader to obtain the signals. The device calibration factor was determined on the accompanying software using the following formula:

$$\text{Device Calibration Factor} = (\text{Signal} - \text{Background}) / \text{Local exposure value}. \quad (1)$$

Subsequently, the dosimeters were annealed for more than 2 h, and background values were measured for the next step. Second, the OSLDs were irradiated with the known local exposure value under the same irradiation condition, then signals from the chips were read out and the sensitivity was obtained on the software using the following formula:

$$\text{Sensitivity} = \text{Local exposure value} \times \text{Device Calibration Factor} / \text{Signal}. \quad (2)$$

Third, after the background was read out, OSLDs were irradiated with the known local exposure value under the same irradiation condition once again, and signals were obtained. The system calibration factor was computed as a conversion when reference field was given using the following formula:

$$\text{System Calibration Factor} = \frac{\text{Reference exposure value} \times \text{Local exposure signal}}{\text{Reference exposure signal} \times \text{Local exposure value}}. \quad (3)$$

From the calibration, the actual dose value is represented as follows:

$$\text{Actual dose value} = \text{Signal} \times \frac{1}{\text{Device Calibration Factor} \times \text{Sensitivity} \times \text{System Calibration Factor}} \quad (4)$$

After calibration, dose verification was performed. The remaining dosimeters, which were implemented in field mode, were irradiated with a particular dose value to obtain the sensitivity, and by the next irradiation, the actual dose was calculated according to the above formula. Then the deviation was compared between the actual dose and known dose. Therefore, the aforementioned dose verification procedure in this study yielded a measurement uncertainty of $\pm$ 5% for the dosimeters.

2.B. Solid water phantom

The Unity system (Elekta, Stockholm, Sweden) comprises a 7 MV flattening filter-free (FFF) ($TPR_{20,10} = 0.703$) Linac and a 1.5 T MRI scanner (Philips, Best, The Netherlands). The magnetic field is oriented along the craniocaudal patient axis perpendicular to the primary beam, and the coordinate system is presented as shown in Fig. 1(a). Homogeneous solid water slabs, with various depths, were stacked to form a cubic solid water phantom (40 × 40 × 14 cm) positioned on the treatment couch.

2.B.1. Solid water phantom setup

To further reduce the setup errors, specific important details were emphasized as follows:

A tungsten ball was used on the center of the solid water phantom at the surface and irradiated at a gantry angle of 0°; frontal images were acquired by the MV imaging controller software (MVIC). The location of the phantom was adjusted and determined by comparing deviations in the center of the small tungsten ball with respect to the treatment isocenter. Marking the phantom edge in black lines, the phantom setup can be accurately reproduced.

Then a tungsten ball was irradiated at gantry angles of 0° and 90°, and frontal and lateral images were acquired by MVIC to validate the isocenter at the center of the phantom surface. Hence, the treatment isocenter was confirmed and marked by a cross, along with the marked edge of a 15 × 15 cm^2 irradiation field in Fig. 1(b).

At the same time, according to the treatment isocenter and marked edge of the irradiation field, each dosimeter was arranged in a line using a scale. Due to the short distance (1 cm) between the measurement points resulting from the small physical size of the dosimeter, the other dosimeters were located next to each other shown in Fig. 1(b). The entire measuring distance is 10 cm in each direction.

2.B.2. Measurements

A cubic solid water phantom with OSLDs on the surface was vertically irradiated by MR-Linac, where OSLDs were arranged out of the beam edges in four directions. The center of first dosimeter for each direction was located 0.5 cm from the beam edge. At a gantry angle of 0° (beam vertical to the phantom), source-to-surface distance of 133.5 cm (SSD), and field size of 10 × 10 cm^2, 200 monitor units (MU) were delivered, which corresponds to 1.67 Gy at a depth of 9.7 cm in the water phantom. Next, the field size was changed to 5 × 5 cm^2, 15 × 15 cm^2, and 20 × 20 cm^2, and the same measurements were performed. Each irradiation was repeated five times and the data from the OSLD measurements were averaged.

2.C. Anthropomorphic phantom

The anthropomorphic adult phantom (ATOM, Computerized Imaging Reference System Inc., Virginia, USA) consists of serial horizontal sections, each 25 mm thick, drilled with thru-holes 5 mm in diameter, and alignment nylon pins stitched together to reduce air gaps. It can simulate the shape of the actual patient and has specific internal organs with solid plugs for holding myOSLchips.

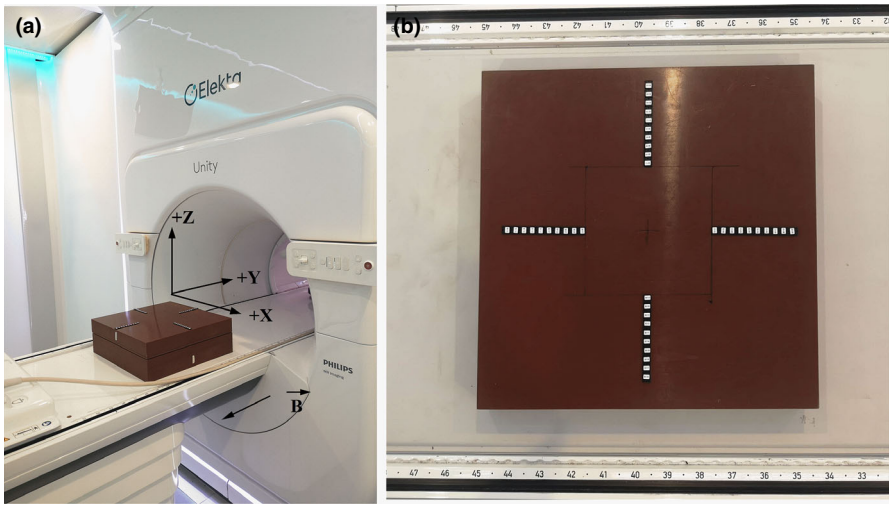

FIG. 1. (a) Coordinate system and the magnetic field orientation are marked by arrows. (b) Solid water phantom (40 × 40 cm) irradiation with optically stimulated luminescence dosimeters ranged out of field of 1.5T MR-Linac at the field size of 15 × 15 cm^2 in four directions. [Color figure can be viewed at wileyonlinelibrary.com]

2.C.1. Simulation setup and treatment planning

Before scanning, the OSLDs were placed on the surface of emulational OAR (e.g., eyes, thyroid, breasts, and testes) of the phantom, locations of which were specific to those of internal organs. This ensures the repeatability of each measurement and improves the accuracy of the TPS dose calculation of the corresponding position.[30] Three scan reference points, aligned to a specific couch index, were marked to achieve stable and reproducible positioning. Then, the computed tomography (CT) simulator was used with a slice thickness of 3 mm, and the CT simulated images were transferred to the Monaco treatment planning system. To simulate specific anatomical sites (head, thoracic, and pelvic), the size of the PTVs was uniformly set to 5 × 5 × 5 cm^3. The PTV of the head was located in slices 2 and 3, that of the thoracic was located in slices 14 and 15, and that of the pelvic was located in slices 34 and 35, as shown in Fig. 2. For each treatment site, 4 equally weighted treatment fields, with gantry angles of 0°, 90°, 180° and 270° were designed, and a prescribed dose of 2000 cGy in 1 fraction was delivered to the target volume of 125 cm^3. The field aperture was set using only collimator jaws to design the three-dimensional conformal radiotherapy (3DCRT) planning. The coverage dose was rescaled to cover 90 % of the target volume to maintain a similar plan quality. The SSD for head, thoracic, and pelvic irradiations using Unity were 135.37, 134.38, and 134.65 cm, respectively. The MR body coil was added in the TPS manually and utilized in each treatment. Before irradiation, gamma analysis using 3%/3 mm pass criteria was performed and points of agreement were over 95 % for the plans of different sites.

2.C.2. Measurements

Given the absence of a cross-laser system and unavailability of a magnetic resonance signal for the anthropomorphic phantom, the position of the center of the small tungsten ball and the PTV isocenter were compared online by MVIC to verify the PTV isocenter and further reduce the setup error before each measurement.

First, during the thoracic treatment, the phantom was adjusted in the supine position on the treatment couch and irradiated with OSLDs lined up at different measurement points, from the beam edge along the central axis as indicated by the blue line in Fig. 2(a). Second, the OSLDs were placed on the surface of the emulational OARs (e.g., eyes, thyroid, breasts, and testes). The phantom was then consecutively irradiated at different radiotherapy sites. As these are some of the most radiosensitive organs, measured surface doses cannot be equivalent to the actual internal doses in the organs, which need to be measured in comparison with the surface dose. Therefore, by inserting myOSLchips into solid plugs, the out-of-field dose of internal simulated OARs were measured.

The same plan of a 5 × 5 cm^2 field size and four orthogonal treatment fields without a multileaf collimator (MLC) for each anatomical site was created to be delivered to the 6 MV FFF ($TPR_{20,10}$ = 0.655) VitalBeam accelerator (Varian Medical Systems Palo Alto, CA). Experiments were conducted in the same way as described above. The SSD for head, thoracic, and pelvic irradiations using VitalBeam were 90.4, 89.4, and 89.6 cm, respectively.

For all measurements, each irradiation was repeated five times and the data from the OSLD measurements were averaged.

2.C.3. TPS dose calculation

Out-of-field dose calculations were performed using the Monaco TPS (V5.40.01, Elekta AB, Stockholm, Sweden) with GPUMCD for 3DCRT treatments. The volume of the dosimeter (1 × 1 × 0.2 cm) was outlined to be approximately 0.2 cm^3 in the TPS calculation. A dose uncertainty of 1 % was set and a 2.0 mm calculation grid size was adopted. The average dose of check points were calculated by TPS

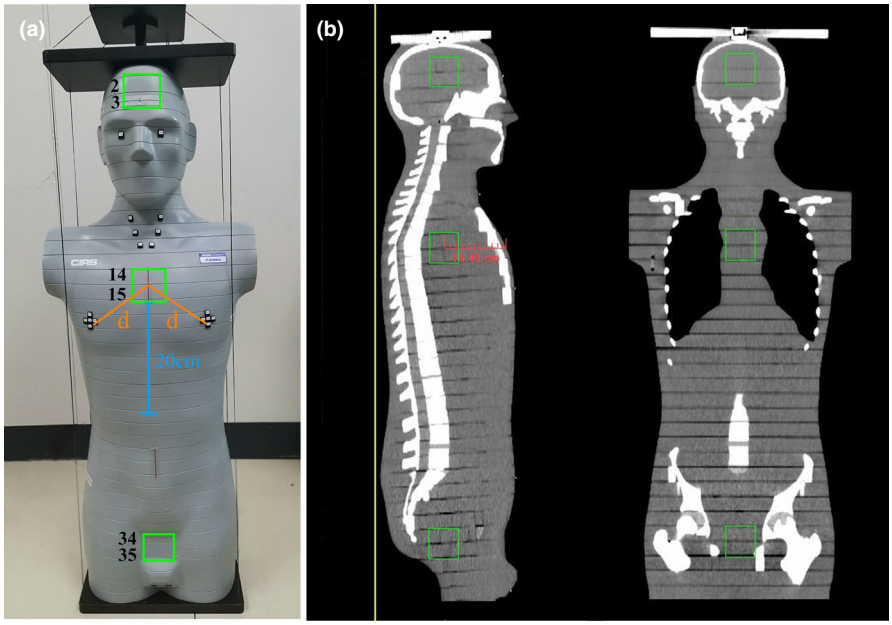

FIG. 2. (a) Photograph of an anthropomorphic phantom with optically stimulated luminescence dosimeters affixed to the surface of its radiosensitive organs. Yellow line "d" was marked as a distance from the planning target volume (PTV) isocenter to the interest points. (b) Locations of outlined PTVs of different treatment sites in the sagittal and coronal planes. [Color figure can be viewed at wileyonlinelibrary.com]

based on the dosimeter delineation. The locations of surface check points and internal simulated OARs were marked as interest points with three-dimensional coordinates. Then, the distances from the PTV isocenter to the interest points were calculated. The TPS calculated dose were compared with the OSLD measurements to determine the out-of-field dose calculation deviation.

3. RESULTS

3.A. Solid water phantom measurements

For the measurements of the solid water phantom, the discrete point doses were connected to a curve. The surface dose values in the X- and Y-directions for the varying field sizes of 5×5 cm^2, 10×10 cm^2, 15×15 cm^2, and 20×20 cm^2 are shown in Fig. 3. As the distance from the beam edge to the distal side of each direction varies, the surface dose was observed for the same field size; the curve exhibits a nearly symmetrical declining distribution within a narrow range, and a sharp decrease in the dose is observed primarily within 1 cm of the beam edge. As the field size increases, the dose increases consistently. For the 10×10 cm^2 field size, the out-of-field surface dose measured on MR-Linac varied from 0.59% to 4.82% of maximum dose and varied from 0.57% to 5.29% of maximum dose longitudinally. For the 5×5 cm^2 field size, the out-of-field surface dose measured on MR-Linac varied from 0.16% to 4.38% of the prescribed dose laterally and varied from 0.14% to 4.40% of maximum dose longitudinally. For the 20×20 cm^2 field size, the out-of-field surface dose measured on MR-Linac varied from 1.76% to 7.02% of maximum dose laterally and varied from 1.41% to 8.56% of maximum dose longitudinally. In conclusion, at different field sizes (5×5 to 20×20 cm^2) and distance (1 to 10 cm) to beam edge, the out-of-field surface dose measured on MR-Linac varied from 0.16 % (10 cm to 5×5 cm^2 edge) to 7.02 % (1 cm to 20×20 cm^2 edge) of maximum dose laterally, and varied from 0.14 % (10 cm to 5×5 cm^2 edge) to 8.56 % (1 cm to 20×20 cm^2 edge) of maximum dose longitudinally.

3.B. Anthropomorphic phantom measurements

3.B.1. Thoracic treatment

Several point doses, from the beam edge in the thoracic, were measured using MR-Linac (Unity) and conventional linac (VitalBeam). In Fig. 4, the surface dose measured using Unity in the thoracic varied from 0.17 % to 2.67 % of prescribed dose within 20 cm from the beam edge. The surface dose measured using VitalBeam in the thoracic varied from 0.17 % to 3.08 % of prescribed dose within 20 cm from the beam edge. Within 5 cm from the beam edge, the measured doses using VitalBeam were higher than those using Unity. For distances more than 5 cm from the beam edge, the measured doses using VitalBeam were lower than those using Unity.

3.B.2. Surface and internal dose

OSLDs were placed on the surfaces of the radiosensitive organs (eyes, thyroid, breasts, and testes) of the phantom. The measured dose of surface check points for different sites (head, thoracic, and pelvic) on the Unity and VitalBeam systems is listed in Table I. A dose of <0.5 cGy was considered too small to be significant and as a result, less reliable. The anatomical location of the target volume plays a dominant

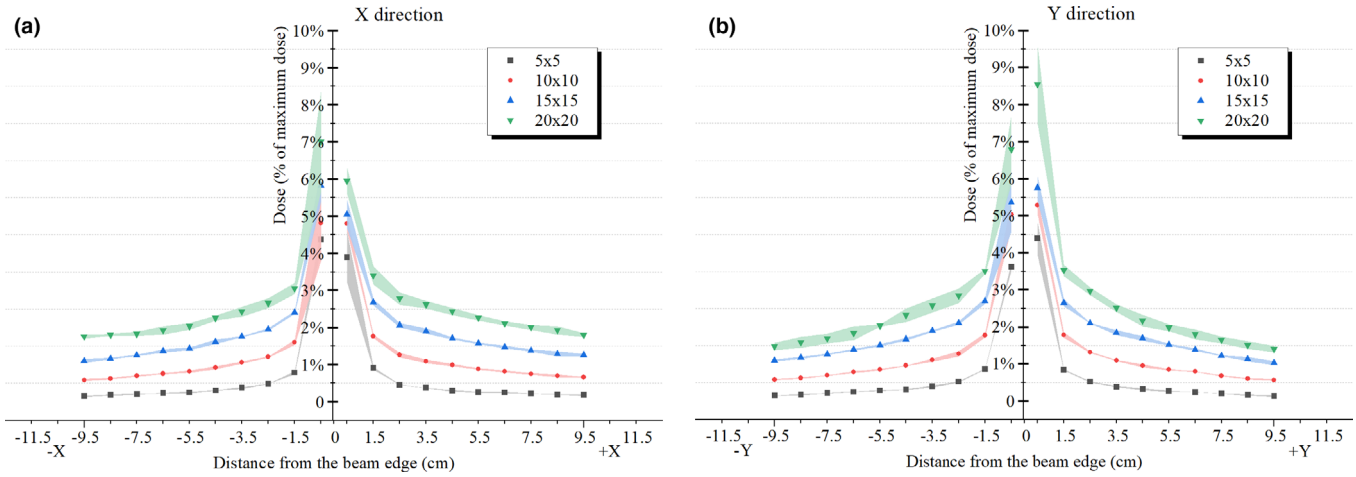

FIG. 3. Point doses measured on MR-Linac at different field sizes and distance from the beam edge on the surface of solid water phantom on (a) X (lateral) and (b) Y (longitudinal) directions. The line thickness indicates the standard deviation of multiple measurements. [Color figure can be viewed at wileyonlinelibrary.com]

role in the out-of-field dose of surface check points. Radiosensitive organs, in close proximity to the target volume, are exposed to a higher dose. The out-of-field dose of the surface check points, near the treatment field, for different treatment sites was no more than 1.45% of the prescribed dose. Compared to the VitalBeam, MR-Linac delivered 20%, 19%, and 21% higher average out-of-field dose on surface check points at head, thoracic, and pelvic irradiations, respectively.

Table II presents the measured doses of internal emulational OARs at different treatment sites using Unity and VitalBeam. Compared to the conventional linac, MR-Linac delivered 42%, 37%, and 9% higher average out-of-field dose on internal simulated OARs of the anthropomorphic phantom at head, thoracic, and pelvic irradiations, respectively.

3.B.3. TPS dose calculation

The ratio of the TPS-calculated dose to the OSLD-measured dose for both surface and internal of the emulational OARs was plotted as a function of distance from the PTV isocenter to dosimeter for the head, thoracic, and pelvic treatment plans using Unity. As shown in Fig. 5(a), the values of D_{TPS}/D_{OSLD} ranged from 65 % (35 % underestimation of dose in TPS) to 370 % (270 % overestimation of dose in TPS), including measurements on the surface and in the phantom. The farther the radiosensitive organ is from the target volume, the greater the ratio of the TPS-calculated dose to the OSLD-measured dose. This in turn results in a greater overestimation of the TPS. Compared to the OSLD-measured data, the Monaco TPS tended to overestimate the out-of-field dose of OARs at 0–2% isodose area on both surface and internal check points. The underestimation was found to be 0–35% at 2–5% isodose area on both the surface and internal check points of the thoracic irradiation.

It was shown that the underestimation gets greater within the distance of 10 to 20 cm from the PTV isocenter to dosimeter using both Unity and VitalBeam. At the distances far from the treatment field, the out-of-field dose of TPS calculation using VitalBeam became constant and relatively small.

For the thoracic irradiation, Fig. 6 depicts the comparison of the 2% and 5% isodose lines using Unity and VitalBeam. The underestimated out-of-field check points using Unity were from the thyroid and breasts, which were within the 2% and 5% isodose ranges in Fig. 6(a). In addition, an extra dose from the chin to the geisoma in the magnetic field was observed, and the dose distribution of the isodose line on the MR-Linac (Unity) was more dispersed than that on the conventional linac (VitalBeam).

4. DISCUSSION

In this study, we investigated the general out-of-field dose distribution in the presence of the magnetic field on a solid water phantom using OSLDs. The out-of-field doses, on both surface and internal of the emulational OARs, were measured. We then compared the results with the measured data from the conventional linac. Relevant dosimetry data are highly recommended to make critical clinical decisions on the out-of-field organs, and the necessity to investigate the potential risks is emphasized for radiation protection.

BeO material is considered as a reliable and suitable OSLD chip for out-of-field dose measurement. The average energy outside the treatment field is much lower, typically between 0.2 and 0.6 MeV.[31,32] According to AAPM TG-158,[33] a dosimeter with a higher effective atomic number (Z_{eff}) than that of tissue will overrespond to this softer radiation. Compared with other materials (such as Al_2O_3:C with Z_{eff} of 11.3), BeO sensitive material utilized as OSLD chips as in this study has a lower effective atomic number (Z_{eff} = 7.2) and near water (Z_{eff} = 7.4) equivalence, and thus is less overresponsive to the softer radiation. As Sarigul et al.[34] observed, BeO chips are energy independent at energies higher than 150 kv (105 keV mean photon energy). Without considering the effect of the number of beam angles on the

TABLE I. Surface dose measurement comparison of radiosensitive organs of different treatment sites on the Unity and VitalBeam (abbreviation for VB).

	Head irradiation			Thoracic irradiation			Pelvic irradiation		
Organ	D_{Unity} (cGy) (Mean ± SD)	D_{VB} (cGy) (Mean ± SD)	D_{Unity}/D_{VB}	D_{Unity} (cGy) (Mean ± SD)	D_{VB} (cGy) (Mean ± SD)	D_{Unity}/D_{VB}	D_{Unity} (cGy) (Mean ± SD)	D_{VB} (cGy) (Mean ± SD)	D_{Unity}/D_{VB}
eye_R (5)*	24.92 ± 0.31	21.34 ± 0.26	1.17	4.90 ± 0.01	2.90 ± 0.09	1.69	<0.5	<0.5	–
eye_L (5)	23.64 ± 0.27	21.37 ± 0.29	1.11	3.85 ± 0.05	3.18 ± 0.09	1.21	<0.5	<0.5	–
thyroid_R (10)	5.62 ± 0.18	5.44 ± 0.21	1.03	16.71 ± 0.23	13.73 ± 0.19	1.22	<0.5	<0.5	–
thyroid_L (10)	5.62 ± 0.17	5.25 ± 0.12	1.07	15.61 ± 0.07	14.34 ± 0.30	1.09	<0.5	<0.5	–
thyroid_R (11)	4.73 ± 0.12	4.59 ± 0.11	1.03	21.13 ± 0.47	18.86 ± 0.36	1.12	<0.5	<0.5	–
thyroid_L (11)	4.60 ± 0.14	4.54 ± 0.12	1.01	20.79 ± 0.79	18.92 ± 0.23	1.10	<0.5	<0.5	–
thyroid_R (12)	4.07 ± 0.12	3.39 ± 0.06	1.20	28.06 ± 0.52	24.65 ± 0.42	1.14	<0.5	<0.5	–
thyroid_L (12)	4.20 ± 0.15	3.43 ± 0.03	1.22	29.03 ± 0.49	26.22 ± 0.31	1.11	<0.5	<0.5	–
breast_R up (17)	1.17 ± 0.07	0.93 ± 0.02	1.26	17.23 ± 0.27	14.37 ± 0.12	1.20	0.56 ± 0.01	0.54 ± 0.02	1.04
breast_R down (17)	0.91 ± 0.07	0.69 ± 0.02	1.32	15.15 ± 0.42	11.91 ± 0.30	1.27	0.86 ± 0.03	0.59 ± 0.02	1.46
breast_R left (17)	1.06 ± 0.02	0.77 ± 0.00	1.38	16.01 ± 0.44	13.76 ± 0.52	1.16	0.63 ± 0.01	0.55 ± 0.02	1.15
breast_R right (17)	1.04 ± 0.03	0.78 ± 0.02	1.33	16.18 ± 0.51	12.88 ± 0.47	1.26	0.72 ± 0.04	0.55 ± 0.01	1.31
breast_R middle (17)	1.01 ± 0.02	0.78 ± 0.02	1.29	16.58 ± 0.10	12.59 ± 0.51	1.32	0.60 ± 0.03	0.56 ± 0.02	1.07
breast_L up (17)	1.13 ± 0.05	0.95 ± 0.02	1.19	16.12 ± 0.39	15.19 ± 0.22	1.06	0.56 ± 0.02	0.52 ± 0.02	1.08
breast_L down (17)	0.90 ± 0.05	0.70 ± 0.02	1.29	15.00 ± 0.48	12.59 ± 0.46	1.19	0.90 ± 0.05	0.58 ± 0.02	1.55
breast_L left (17)	0.99 ± 0.03	0.85 ± 0.01	1.16	15.09 ± 0.33	13.58 ± 0.24	1.11	0.79 ± 0.03	0.61 ± 0.01	1.30
breast_L right (17)	1.11 ± 0.04	0.82 ± 0.03	1.35	15.60 ± 0.21	14.19 ± 0.28	1.10	0.69 ± 0.03	0.52 ± 0.01	1.33
breast_L middle (17)	1.00 ± 0.02	0.79 ± 0.03	1.27	15.96 ± 0.20	13.89 ± 0.27	1.15	0.62 ± 0.05	0.53 ± 0.03	1.17
testic_R (38)	<0.5	<0.5	–	<0.5	<0.5	–	17.79 ± 0.42	17.13 ± 0.30	1.04
testic_L (38)	<0.5	<0.5	–	<0.5	<0.5	–	18.15 ± 0.30	17.09 ± 0.24	1.06
average value			1.20			1.19			1.21

*Number in the parentheses indicates the slice number marking the locations of the radiosensitive organ.

surface dose, a 3DCRT treatment plan with four beam angles was employed, and the OSLD chips with plastic holders were uniformly selected.[35]

In Fig. 3, a sharp decrease is observed within 1 cm of the beam edge, where the sensitive volume of the OSLDs, which converts the obtained signals to the mean dose value, is just within the limited range. The surface dose decreases as the distance from the beam edge increases and increases as the field size expands. This is because there are more photons owing to the larger irradiation volume, which leads to more scattering contribution of patient scatter.[36,37]

In the first part of the anthropomorphic phantom measurements, several point doses in the thoracic were measured using Unity and VitalBeam. Within the distance of 5 cm from the beam edge, patient scatter comprises a large fraction of the total out-of-field dose in the FFF mode when close to the treatment field,[38] and VitalBeam ($TPR_{20,10} = 0.655$) has a lower energy than Unity ($TPR_{20,10} = 0.703$) exhibiting more patient scatter with the same treatment technique.[39] Therefore, it is observed that the measured point doses were higher using VitalBeam than those using Unity within 5 cm from the beam edge. Beyond 5 cm, the scattered dose from the linac head design and electrons generated in the air may increase the dose in the case of Unity.

For the thoracic irradiation, the extra dose from the chin to the geisoma in the magnetic field was observed to be the result of the ESE, as investigated by Nachbar et al.[12] As mentioned above, the electron return effect cannot be ignored in practical clinical treatment.[12] To reduce the device-specific differences for the MR-Linac and the conventional linac (as Nachbar noted[40]) as much as possible, we employed the 3DCRT technique for the same field size with no MLC to ensure the same target coverage and therapeutic effect on the anthropomorphic phantom. Therefore, the differences in the out-of-field dose between the MR-Linac and the conventional linac are mainly beam energy, Linac head design, SSD, and the magnetic field. As Covington et al. noted, the measured peripheral dose in the FFF mode decreased with increasing energy for all field sizes and depths[41]; thus, it can be concluded that the out-of-field dose for 6 MV FFF VitalBeam ($TPR_{20,10} = 0.655$) was slightly higher than that of 7 MV FFF Unity ($TPR_{20,10} = 0.703$). However, given that this study focused on the treatment plans of four beam angles, instead of a single beam, this result may not be obvious and applicable. It is important to note that the Linac head design, including the MR cryostat and MR body coil, are the source of a small amount of scattered radiation.[42] In addition, the effect of the magnetic field cannot be ignored. Although the number of electrons reaching the surface of the phantom decreased due to a larger SSD,[43] the trajectories of secondary electrons were deflected by the magnetic field and therefore the secondary electrons may increase the out-of-field dose.

As indicated in AAPM TG-158,[33] if a dosimeter is placed on the patient surface, it should be covered by a bolus of

TABLE II. Doses measured for internal simulated radiosensitive organs at different treatment sites using Unity and VitalBeam (abbreviation for VB).

	Head irradiation			Thoracic irradiation			Pelvic irradiation		
Organ	D_{Unity} (cGy) (Mean ± SD)	D_{VB} (cGy) (Mean ± SD)	D_{Unity}/D_{VB}	D_{Unity} (cGy) (Mean ± SD)	D_{VB} (cGy) (Mean ± SD)	D_{Unity}/D_{VB}	D_{Unity} (cGy) (Mean ± SD)	D_{VB} (cGy) (Mean ± SD)	D_{Unity}/D_{VB}
eye (5)*	23.68 ± 0.47	21.68 ± 0.32	1.09	3.35 ± 0.08	2.16 ± 0.04	1.55	<0.5	<0.5	–
thyroid (11)	4.34 ± 0.14	3.28 ± 0.09	1.32	22.57 ± 0.58	18.84 ± 0.33	1.20	<0.5	<0.5	–
breast_L (17)	0.91 ± 0.04	0.58 ± 0.01	1.57	17.96 ± 0.65	13.32 ± 0.17	1.35	0.58 ± 0.02	0.53 ± 0.01	1.09
breast_R (17)	0.95 ± 0.03	0.56 ± 0.02	1.70	18.02 ± 0.67	13.07 ± 0.43	1.38	0.59 ± 0.02	0.51 ± 0.01	1.16
testic (38)	<0.5	<0.5	–	<0.5	<0.5	–	20.57 ± 0.71	20.32 ± 0.53	1.01
average value			1.42			1.37			1.09

*Number in the parentheses indicates the slice number marking the locations of the radiosensitive organ.

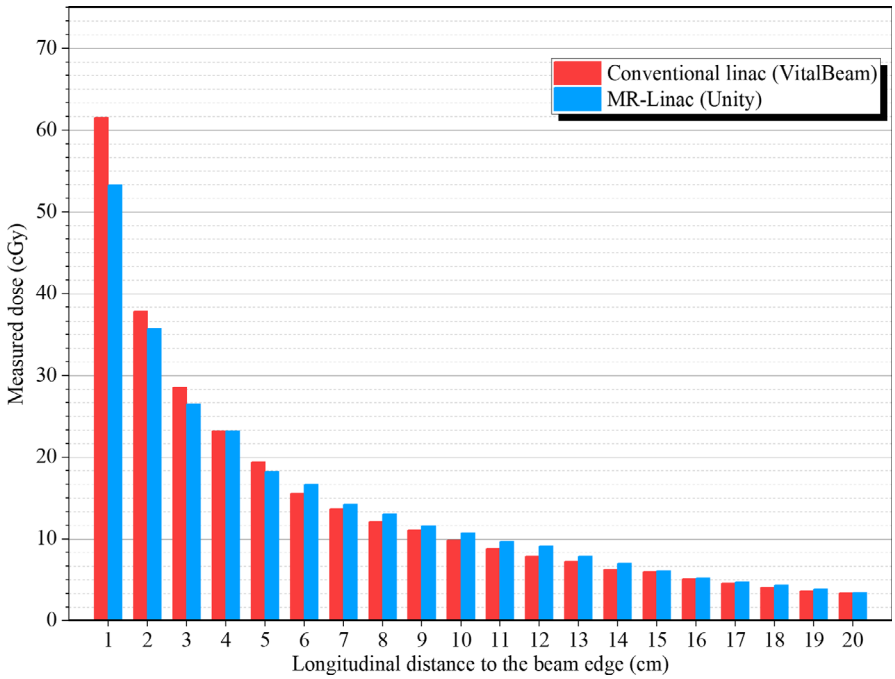

FIG. 4. Measured point dose at distances from the beam edge of thoracic 125 cm^3 20 Gy irradiation at the surface of the anthropomorphic phantom on conventional linac (VitalBeam) and MR-Linac (Unity), respectively. [Color figure can be viewed at wileyonlinelibrary.com]

certain thickness if the superficial dose estimate is desired. Otherwise, it will overestimate the dose. In this study, the superficial and internal doses to radiosensitive organs (eyes, thyroid, breasts, and testes) were of particular interest; hence, the bolus was not used in the measurement.

From Tables I and II, compared to the conventional linac, MR-Linac delivered higher average out-of-field dose on surface check points and internal simulated OARs of the anthropomorphic phantom at head, thoracic, and pelvic irradiations. The slight dose difference between two linacs may be explained as follows: for most radiosensitive organs near the treatment region, secondary electrons from the patient may escape into the air, make a spiral motion along the magnetic field, and be deposited back to the surface of the patient outside the target volume.[12,14] Moreover, contaminant electrons, generated from the Linac head or air, may be swept out of the irradiation field, similarly spiral toward the magnetic field poles, and be trapped on the surface of the patient away from the treatment region.[14] It has been found that the measured dose could be lower when irradiated using the MR-Linac for the radiosensitive organs close to the target volume, as shown in Fig. 4. However, it may be different for the thyroid near the target in the thoracic irradiation. Owing to the ESE in the magnetic field, electrons move in an inferior–superior direction along the central axis of the phantom and finally deposit on the surface of the neck, resulting in an increase in the irradiated dose to the thyroid.

For the out-of-field dose of the surface check points and internal simulated OARs, there is a slight dose difference between the measured and calculated dose of the TPS. As the distance from the beam edge increases, the ratio of TPS-calculated and OSLD-measured dose also increases. This suggests that the out-of-field dose of the Monaco TPS calculation was inaccurate. During irradiations at different sites,

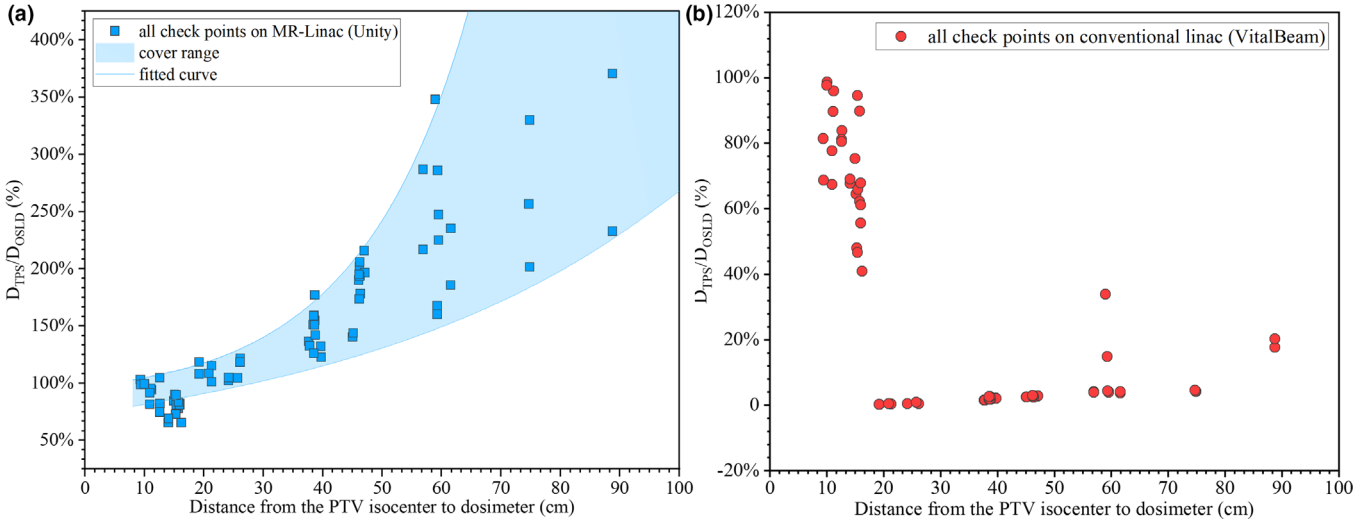

FIG. 5. Ratio of the treatment planning system-calculated dose to the optically stimulated luminescence dosimeters-measured dose plotted as a function of distance from the planning target volume isocenter to dosimeter for all check points on both the surface and internal organs at risk using Unity and VitalBeam, respectively.

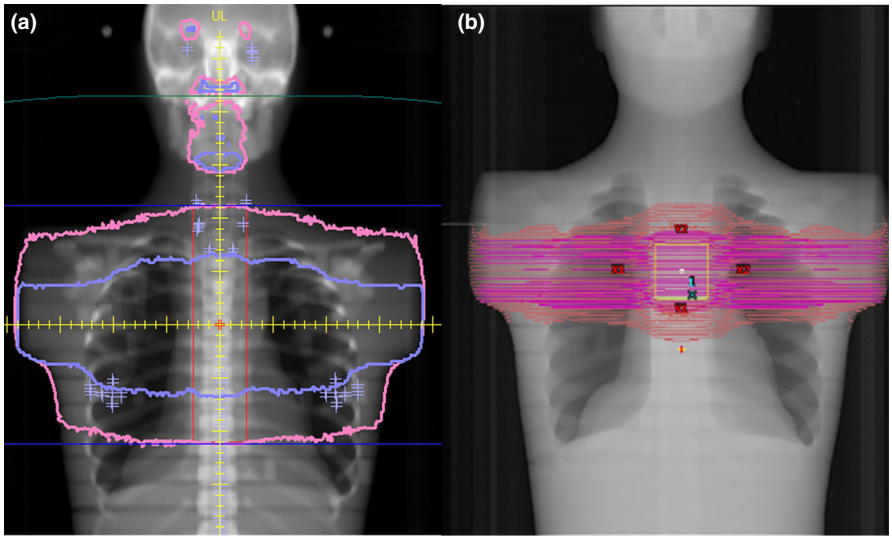

FIG. 6. Comparison between isodose lines of the same thoracic case. Light- and dark-colored isodose levels represent 2 % and 5 % isodose lines, respectively. (a) Beam's eye view at gantry angle of 0° on MR-Linac (Unity). (b) Beam's eye view at gantry angle of 0° on conventional linac (VitalBeam).

the measured dose at check points far from the treatment field was extremely small (less than 0.5 cGy), resulting in a very large D_{TPS}/D_{OSLD}. In this study, the underestimation of out-of-field dose calculation of Monaco TPS within 2% and 5% isodose ranges is similar to the experimental results presented by Sánchez-Nieto et al.[44] The overestimation at 0–2 % isodose area became more severe with increasing distance from the beam edge. Out-of-field dose of TPS calculation on VitalBeam was underestimated over the check points in accordance with Howell et al.'s findings.[29] This indeed reveals the concern that out-of-field doses may have been ignored; therefore, accurate dose measurements are necessary to evaluate the long-term adverse effects associated with low-dose exposures as well as potentially reduce the risk of secondary cancer.

The results of this study were specific to the Monaco TPS version 5.40.01 and Varian VitalBeam Linac system and to the Elekta Unity. In general, the deviations reported in this study are for surface and internal of simulated OARs at a large off-axis distance. For the solid water phantom measurements, it should be considered that OSLDs placed between the water phantom stacks may have a large position error, and the remaining air gap may increase the actual dosimetry data. Therefore, the impact of depth on the out-of-field dose was not assessed in the study, and the characterization of depth remains to be considered as future work. This study was conducted with the limited number of checkpoints, and more check points need to be considered in the future to evaluate the accuracy of Monaco TPS in out-of-field dose calculation. Also, radiation exposure is a concern for other OARs under

various conditions and not just radiosensitive organs. It is suggested that measurements be made on the basis of specific phantom experiments.

5. CONCLUSION

The quantified out-of-field dose distribution for a perpendicular MR-Linac was measured using OSLDs. Compared to the conventional linac, MR-Linac has the same out-of-field dose distribution. This study makes a solid contribution to the current literature on out-of-field dosimetry of MR-Linac and provides a reference for high-precision Monte Carlo simulations. However, considering the absolute dose values, MR-Linac delivered relatively higher out-of-field dose on both surface and internal OARs. Additional radiation shielding to patients undergoing MR-Linac may provide protection from out-of-field exposure.

ACKNOWLEDGMENTS

Funding was provided in part by the National Natural Science Foundation of China (grant numbers 81671785, 81530060 and 81874224), the National Key Research and Development Program of China (grant number 2016YFC0105106), the Foundation of Taishan Scholars (No.tsqn201909140, ts20120505), and the Shandong Provincial Natural Science Foundation (ZR2016HQ09, ZR2020LZL001).

CONFLICT OF INTEREST

The authors have no conflict of interest to disclose.

DATA AVAILABILITY STATEMENT

Data are available as supplemental files associated with the online journal article.

[a)]Authors to whom correspondence should be addressed. Electronic mails: zhujian@sdfmu.edu.cn, csp6606@sina.com.

REFERENCES

1. Dawson LA, Jaffray DA. Advances in image-guided radiation therapy. *J Clin Oncol*. 2007;25:938–946.
2. Perks JR, Lehmann J, Chen AM, Yang CC, Stern RL, Purdy JA. Comparison of peripheral dose from image-guided radiation therapy (IGRT) using kV cone beam CT to intensity-modulated radiation therapy (IMRT). *Radiother Oncol*. 2008;89:304–310.
3. Siewerdsen JH, Jaffray DA. Cone-beam computed tomography with a flat-panel imager: magnitude and effects of x-ray scatter. *Med Phys*. 2001;28:220–231.
4. Raaymakers BW, Jürgenliemk-Schulz IM, Bol GH, et al. First patients treated with a 1.5 T MRI-Linac: Clinical proof of concept of a high-precision, high-field MRI guided radiotherapy treatment. *Phys Med Biol*. 2017;62:L41–L50.
5. Acharya S, Fischer-Valuck BW, Kashani R, et al. Online magnetic resonance image guided adaptive radiation therapy: First clinical applications. *Int J Radiat Oncol Biol Phys*. 2016;94:394–403.
6. Liney GP, Whelan B, Oborn B, Barton M, Keall P. MRI-linear accelerator radiotherapy systems. *Clin Oncol*. 2018;30:686–691.
7. Kirkby C, Murray B, Rathee S, Fallone BG. Lung dosimetry in a linac-MRI radiotherapy unit with a longitudinal magnetic field. *Med Phys*. 2010;37:4722–4732.
8. Kubota T, Araki F, Ohno T. Impact of inline magnetic fields on dose distributions for VMAT in lung tumor. *Phys Med*. 2019;59:100–106.
9. Raaijmakers AJ, Raaymakers BW, van der Meer S, Lagendijk JJ. Integrating a MRI scanner with a 6 MV radiotherapy accelerator: Impact of the surface orientation on the entrance and exit dose due to the transverse magnetic field. *Phys Med Biol*. 2007;52:929–939.
10. Cusumano D, Teodoli S, Greco F, et al. Experimental evaluation of the impact of low tesla transverse magnetic field on dose distribution in presence of tissue interfaces. *Phys Med*. 2018;53:80–85.
11. Raaijmakers AJ, Raaymakers BW, Lagendijk JJ. Integrating a MRI scanner with a 6 MV radiotherapy accelerator: Dose increase at tissue-air interfaces in a lateral magnetic field due to returning electrons. *Phys Med Biol*. 2005;50:1363–1376.
12. Nachbar M, Mönnich D, Boeke S, et al. Partial breast irradiation with the 1.5 T MR-Linac: First patient treatment and analysis of electron return and stream effects. *Radiother Oncol*. 2020;145:30–35.
13. Park JM, Shin KH, Kim J-I, et al. Air-electron stream interactions during magnetic resonance IGRT: Skin irradiation outside the treatment field during accelerated partial breast irradiation. *Strahlenther Onkol*. 2018;194:50–59.
14. Hackett SL, van Asselen B, Wolthaus JWH, et al. Spiraling contaminant electrons increase doses to surfaces outside the photon beam of an MRI-linac with a perpendicular magnetic field. *Phys Med Biol*. 2018;63:095001.
15. Diallo I, Haddy N, Adjadj E, et al. Frequency distribution of second solid cancer locations in relation to the irradiated volume among 115 patients treated for childhood cancer. *Int J Radiat Oncol Biol Phys*. 2009;74:876–883.
16. Taylor ML, Kron T. Consideration of the radiation dose delivered away from the treatment field to patients in radiotherapy. *J Med Phys*. 2011;36:59–71.
17. Tubiana M. Can we reduce the incidence of second primary malignancies occurring after radiotherapy? A critical review. *Radiother Oncol*. 2009;91:4–15.
18. Guersen J, Cassagnes L, Méchin G, et al. Eye lens irradiation by CT perfusion: Dosimetry and optimization. *Radioprotection*. 2014;49:195–199.
19. Blakely EA, Kleiman NJ, Neriishi K, et al. Radiation cataractogenesis: epidemiology and biology. *Radiat Res*. 2010;173:709–717.
20. Ainsbury EA, Bouffler SD, Dörr W, et al. Radiation cataractogenesis: a review of recent studies. *Radiat Res*. 2009;172:1–9.
21. Majer M, Stolarczyk L, De Saint-Hubert M, et al. Out-of-field dose measurements for 3d conformal and intensity modulated radiotherapy of a paediatric brain tumour. *Radiat Prot Dosimetry*. 2017;176:331–340.
22. Athar BS, Paganetti H. Comparison of second cancer risk due to out-of-field doses from 6-MV IMRT and proton therapy based on 6 pediatric patient treatment plans. *Radiother Oncol*. 2011;98:87–92.
23. Tchistiakova E, Kim A, Song WY, Pang G. MR-safe personal radiation dosimeters. *J Appl Clin Med Phys*. 2017;18:180–184.
24. Bos AJJ. High sensitivity thermoluminescence dosimetry. *Nucl Instrum Methods Phys Res B*. 2001;184:3–28.
25. Sommer M, Jahn A, Henniger J. Beryllium oxide as optically stimulated luminescence dosimeter. *Radiat Meas*. 2008;43:353–356.
26. Spindeldreier CK, Schrenk O, Ahmed MF, et al. Feasibility of dosimetry with optically stimulated luminescence detectors in magnetic fields. *Radiat Meas*. 2017;106:346–351.
27. Huang JY, Followill DS, Wang XA, Kry SF. Accuracy and sources of error of out-of field dose calculations by a commercial treatment planning system for intensity-modulated radiation therapy treatments. *J Appl Clin Med Phys*. 2013;14:4139.
28. Bahreyni Toossi MT, Soleymanifard S, Farhood B, Mohebbi S, Davenport D. Assessment of accuracy of out-of-field dose calculations by TiGRT treatment planning system in radiotherapy. *J Cancer Res Ther*. 2018;14:634–639.
29. Howell RM, Scarboro SB, Kry SF, Yaldo DZ. Accuracy of out-of-field dose calculations by a commercial treatment planning system. *Phys Med Biol*. 2010;55:6999–7008.

30. Zhuang AH, Olch AJ. Validation of OSLD and a treatment planning system for surface dose determination in IMRT treatments. *Med Phys*. 2014;41:081720.
31. Edwards CR, Mountford PJ. Near surface photon energy spectra outside a 6 MV field edge. *Phys Med Biol*. 2004;49:N293–N301.
32. Scarboro SB, Followill DS, Howell RM, Kry SF. Variations in photon energy spectra of a 6 MV beam and their impact on TLD response. *Med Phys*. 2011;38:2619–2628.
33. Kry SF, Bednarz B, Howell RM, et al. AAPM TG 158: Measurement and calculation of doses outside the treated volume from external-beam radiation therapy. *Med Phys*. 2017;44:e391–e429.
34. Sarigul N, Surucu M, Aydogan B. Energy response factor of beo dosemeter chips: a monte carlo simulation and general cavity theory studY. *Radiat Prot Dosimetry*. 2019;185:303–309.
35. Lim-Reinders S, Keller BM, Sahgal A, Chugh B, Kim A. Measurement of surface dose in an MR-Linac with optically stimulated luminescence dosimeters for IMRT beam geometries. *Med Phys*. 2020;47:3133–3142.
36. Kase KR, Svensson GK, Wolbarst AB, Marks MA. Measurements of dose from secondary radiation outside a treatment field. *Int J Radiat Oncol Biol Phys*. 1983;9:1177–1183.
37. Kaderka R, Schardt D, Durante M, et al. Out-of-field dose measurements in a water phantom using different radiotherapy modalities. *Phys Med Biol*. 2012;57:5059–5074.
38. Kry SF, Vassiliev ON, Mohan R. Out-of-field photon dose following removal of the flattening filter from a medical accelerator. *Phys Med Biol*. 2010;55:2155–2166.
39. Ruben JD, Smith R, Lancaster CM, Haynes M, Jones P, Panettieri V. Constituent components of out-of-field scatter dose for 18-MV intensity modulated radiation therapy versus 3-dimensional conformal radiation therapy: a comparison with 6-MV and implications for carcinogenesis. *Int J Radiat Oncol Biol Phys*. 2014;90:645–653.
40. Nachbar M, Mönnich D, Kalwa P, Zips D, Thorwarth D, Gani C. Comparison of treatment plans for a high-field MRI-linac and a conventional linac for esophageal cancer. *Strahlenther Onkol*. 2019;195:327–334.
41. Covington EL, Ritter TA, Moran JM, Owrangi AM, Prisciandaro JI. Technical Report: Evaluation of peripheral dose for flattening filter free photon beams. *Med Phys*. 2016;43:4789.
42. Woodings SJ, Bluemink JJ, de Vries JHW, et al. Beam characterisation of the 1.5 T MRI-linac. *Phys Med Biol*. 2018;63:085015.
43. Yadav G, Yadav RS, Kumar A. Skin dose estimation for various beam modifiers and source-to-surface distances for 6MV photons. *J Med Phys*. 2009;34:87–92.
44. Sánchez-Nieto B, Medina-Ascanio KN, Rodríguez-Mongua JL, Doerner E, Espinoza I. Study of out-of-field dose in photon radiotherapy: A commercial treatment planning system versus measurements and Monte Carlo simulations [published online ahead of print, 2020 Jun 24]. *Med Phys*. 2020;47:4616–4625.